Sensor Review
High-resolution tactile sensor using the deformation of a reflection image
Satoshi Saga, Hiroyuki Kajimoto, Susumu Tachi,

Research article

# High-resolution tactile sensor using the deformation of a reflection image

*Satoshi Saga, Hiroyuki Kajimoto and Susumu Tachi*
Tachi Laboratory, Department of Information Physics and Computing, Faculty of Engineering, Graduate School of Information Science and Technology, The University of Tokyo, Tokyo, Japan

**Abstract**
**Purpose** – The aim of this paper is to create a sensor that can measure the contact status with high-resolution than ever.
**Design/methodology/approach** – This paper proposes a new type of optical tactile sensor that can detect surface deformation with high precision by using the principle of optical lever. A tactile sensor is constructed that utilizes the resolution of a camera to the maximum by using transparent silicone rubber as a deformable mirror surface and taking advantage of the reflection image.
**Findings** – It has been found that the sensor can sense the deformation by the object with 1 percent error rate in simulation. In implementation of this time, the error rate results 10 percent.
**Research limitations/implications** – This sensor can be used with broad applications by combining with other devices. As one of future work, the zero method will be used by using active patterns and get more accurate information.
**Practical implications** – Using the transparent silicone rubbers the sensor enables very simple and low cost and high-resolution detection method. In addition, the simplicity of our sensor results various applications. For example, the transparency makes the sensor a light pathway, so the sensor can be a contactless sensor or an interactive device.
**Originality/value** – The concept of a tactile sensing method is introduced which can utilize the resolution of a camera to the maximum possible extent and can detect surface deformation by using the principle of optical lever.

**Keywords** Sensors, Measurement, Tactile sensors, Image sensors

**Paper type** Research paper



## 1. Introduction

In recent years, with the advancement in robotics, many tactile sensors have been developed to improve force sensation in robots. Several tactile sensors are commercially available in the market, for example, the 6-axis force/torque sensor that can measure the force at one point (BL AUTOTEC LTD, www.bl-autotec.co.jp/english/pdf/bl-sensor.pdf, p. 14). Another sensor can measure the distribution of the contact state or the force distribution (Nitta Corporation, www.nitta.co.jp/english/product/mechasen/sensor/tactile_product_flexi.html).

The disadvantage of these distribution-type force sensors is the number of wirings of sensor units. Each sensor unit is arranged in close proximity to the measurement surface in order to allow a small sensor to be individually distributed, and the wiring that gathers information from a unit is also individually wired. Therefore, a sensor itself cannot prevent deterioration due to the stress of repeated measurements; further, the assembly of the wiring is complicated.

Some optical sensors (Kamiyama *et al.*, 2005; Yamada *et al.*, 2002) such as the distribution-type optical tactile sensor have already been studied. In these sensors, the sensing units and the corresponding wirings from the measurement surface can be eliminated by using a camera. However, as these sensors measure the motion of markers embedded in the elastic body, the sensor resolution, rather than the camera resolution, is determined by the markers. Therefore, the resolution of the camera is not completely utilized.

On the other hand, several techniques that have not been used so far in tactile sensors to measure the shape of an object have been studied. For example, there exists a method that uses the Moire interference fringe pattern or slit light when the object is a diffusive surface (Miike *et al.*, 1995; Baba *et al.*, 2002). In addition, there exists an exact measurement method that uses a laser and a collimator (Yamaguchi *et al.*, 1999). One method uses the specular surface of water (Schultz, 1992). However, in all these methods, it is difficult to improve the time resolution. Therefore, the use of these techniques is limited to the static objects.

In this paper, we examine a sensor that uses an optical lever. An optical lever is a technique that magnifies the displacement by using the characteristics of reflection. The optical lever technique is mostly used in minute domains, such as sample measurements under a microscope (Meyer and Amer, 1988). As another example of the application of the optical lever approach, the deformation of a glass surface was measured in the study (Massig, 2001). The object

The current issue and full text archive of this journal is available at
www.emeraldinsight.com/0260-2288.htm

Sensor Review
27/1 (2007) 35–42
 [ISSN 0260-2288]
[DOI 10.1108/02602280710723451]

measured in this technique is a static glass surface and it is based on a recursive calculation. Moreover, this approach measures the deformation of the glass surface itself and does not measure the contact object. We propose a sensor with a new system that takes advantage of the optical lever and a flexible mirror surface, and measures a reflection image. Owing to the reflection image we can use the full resolution of the camera.

Transparent silicone rubber is used as the flexible mirror surface. Because of the distribution of the refractive index between air and the silicone rubber, the boundary surface has a reflection characteristic similar to that of a mirror surface. We construct a sensor with a flexible mirror surface by using this mirror surface reflection characteristic (Figure 1).

## 2. Principle

We decided to use an optical lever in our sensor. Our aim is to develop a flexible mirror surface by using this optical lever. The sensor detects the deformation of the surface by measuring the displacement via a reflection image from the mirror surface.

### 2.1 Reflection condition

The optical lever technique is mostly used in minute domains, such as sample measurements under a microscope (Meyer and Amer, 1988). By irradiating the tip of cantilevers with lasers and using the reflection characteristics, an optical lever is used to magnify the displacement of the reflection surface.

The sensor uses transparent silicone rubber as the flexible mirror surface. With regard to the boundary between silicone rubber and air (Figure 2), the refractive indices are denoted by $n_r$ and $n_a$, and the refraction angles by $\phi_r$ and $\phi_a$. The notations r and a denote rubber and air, respectively. When the distribution of the refractive index at the boundary of the silicone rubber and air satisfies equation (3), total internal reflection occurs; further, this boundary surface assumes the reflection characteristic of a mirror surface. We design a sensor with a flexible mirror surface by using the above mentioned mirror surface reflection characteristic. By arranging the image pattern, camera, and the transparent silicone rubber as shown in Figure 1, the light diffused from the image pattern is reflected from the silicone rubber boundary and captured by the camera:

$$n_r \sin \phi_r = n_a \sin \phi_a \tag{1}$$

$$\phi_r = \arcsin\left(\frac{n_a}{n_r} \sin \phi_a\right) \tag{2}$$

$$\phi_r > \arcsin\left(\frac{n_a}{n_r}\right) \tag{3}$$

**Figure 1** Section of a sensor: this is the cross section of the sensor. The sensor is in the shape of a triangular pillar

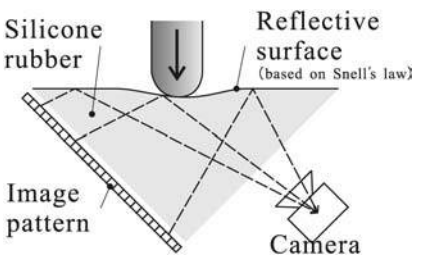


**Figure 2** Snell's law: based on Snell's law, total internal reflection is achieved

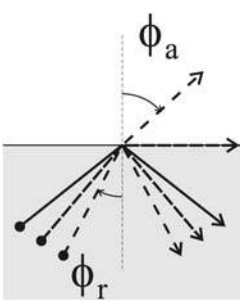


### 2.2 Deformation of the reflection image

In some optical tactile sensors, a camera is used as the optical sensor (Begej, 1984; Kamiyama *et al.*, 2005); the sensor detects the deformation by tracing a marker. However, the resolution of this sensor is limited because of the restriction due to the overlapping of markers. Further we propose a tactile sensor for the new system that makes use of a reflection image in order to utilize the resolution of the camera to the maximum possible extent.

If the contact object touches the silicone rubber, the silicone rubber boundary will be deformed. Consequently, the deformation of the reflection surface occurs, thereby deforming the reflection image of the image pattern. The sensor measures the deformation of the reflection surface by solving an inverse problem using this deformation. Therefore, the entire reflection image contains information; as a result, the resolution of the camera can be utilized to the maximum possible extent. For example, if a checker pattern is used as the pattern surface, not only the lattice points, but also the lattice line contains the deformation information. By using this information, the resolution of the camera can be used. Further utilization of the resolution is explained in Section 6.5. However, in this paper, we have described only the case in when the sensor utilizes the characteristic point of the captured image; it can however, utilize all the points in the captured image in the form of information for reconstruction.

### 2.3 Geometrical optics

We denote the deformed depth of the point $Q_1$ on the reflection surface $q$ by $d$, and the depth displacement between the adjacent points, $Q_1$ and $Q_2$ by $\Delta d$ and the angle at each point on the surface by $\theta$, and the angular displacement between the adjacent points, $Q_1$ and $Q_2$ by $\Delta\theta$. Here, we express $\Delta d$ with $\theta$, and then express $\Delta d$ with known values via $\Delta\alpha$ (defined below).

When the captured pattern is planarly arranged as shown in Figure 3, the surface with this pattern is referred to as the pattern surface $p$. The angle between the pattern surface $p$ and the reflection surface $q$ is represented by $\alpha_0$, while the angle between the captured surface $r$ and the reflection surface $q$ is represented by $\beta_0$. For example, the light diffused from $P_1$ is reflected at $Q_1$, and it reaches $R_1$.

The $x$, $y$, and $z$ axes are shown in Figure 3. $l$ denotes the distant length from $P_0$ in the $y$ direction, and $k$ denotes also the distant length from $P_0$ in the $z$ direction (here, the $z$ axis is

**Figure 3** Geometrical optics: we express $\Delta d$ with known values via $\Delta\alpha$

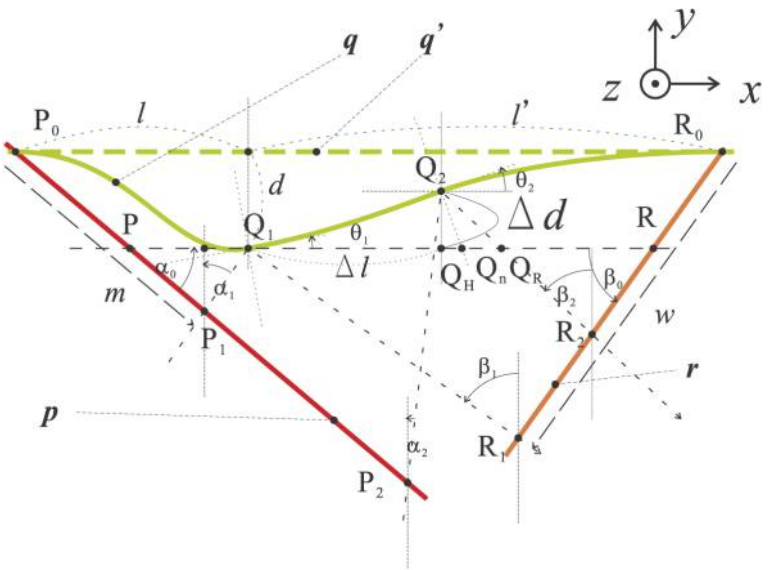


perpendicular to the plane of Figure 3). We assume that after some deformation $Q_1$, which is at a distance $l$ from $P_0$ in $x$ direction, is projected at a distance $d$ and inclined at an angle $\theta_1$ with respect to the surface $q'$ before the deformation. Similarly, after the deformation, $Q_2$, which is $l+\Delta l$ away from $P_0$, is projected at a distance $d+\Delta d$ and inclined at an angle $\theta_2$. Further, we assume that the rays are projected in the following order: $P_1 \rightarrow Q_1 \rightarrow R_1$ and $P_2 \rightarrow Q_2 \rightarrow R_2$. The ray group captured by the camera is assumed to be inclined to the pattern surface at angles $\beta_1$ and $\beta_2$, while it is assumed to be inclined to the captured surface at angles $\alpha_1$ and $\alpha_2$. The symbol $\rightarrow$ denotes the direction of a projected light. Here, we denote $\Delta l$ by $L$ and $\Delta\theta$ by $\Theta$. If the degree of leaning of the reflection surface in $Q_1$ and $Q_2$ changes continually from $\theta_1$ to $\theta_2$, the height displacement $\Delta d$ and the length of $Q_2Q_H$ can be expressed as follows:

$$\Delta d = \int_0^L \tan\left(\theta + \frac{\Theta}{L}l\right)\mathrm{d}l \tag{4}$$

$$= \frac{L}{\Theta}\log\left(\left|\frac{\cos\theta}{\cos(\theta+\Theta)}\right|\right) \tag{5}$$

In addition, based on the symmetry of the incidence angle and the reflection angle at the reflection surface, the following equations are obtained:

$$\angle P_2Q_2Q_H = \angle Q_HQ_2Q_R - 2\angle Q_HQ_2Q_n \tag{6}$$

$$= \beta_2 - 2\theta_2 \tag{7}$$

$$\alpha_2 = \beta_2 - 2\theta_2 \tag{8}$$

Here, the $\angle P_2Q_2Q_H$ denotes the angle between $P_2Q_2$ and $Q_2Q_H$ and $Q_n$ denotes the intersection between the perpendicular from $Q_2$ and the line $PR$. Similarly,

$$\alpha_1 = \beta_1 - 2\theta_1 \tag{9}$$

Next, we express $m = P_0P_1$, $w = R_0R_1$ with $l$. Using the sine theorem in triangle $P_0P_1Q_1$ in Figure 4, which is a part of the spread image of Figure 3, we obtain:

$$\gamma = \arctan\frac{d}{l} \tag{10}$$

$$\frac{\sqrt{l^2+d^2}}{\sin\left(\frac{\pi}{2}-(\alpha_0-\alpha_1)\right)} = \frac{m}{\sin\left(\frac{\pi}{2}-(\alpha_1-\gamma)\right)} \tag{11}$$

$$m = \sqrt{l^2+d^2}\,\frac{\cos(\alpha_1-\gamma)}{\cos(\alpha_1-\alpha_0)} \tag{12}$$

Similarly, we have:

$$\gamma' = \arctan\frac{d}{l'} \tag{13}$$

$$w = \sqrt{l'^2+d^2}\,\frac{\cos(\beta_1-\gamma')}{\cos(\beta_1-\beta_0)} \tag{14}$$

equations (10), (12)–(14) indicate that the $m$ and $w$ values can be expressed by the known values and measured values from the camera.

### 2.4 Reconstruction of the reflection surface

The sensor can measure $m$, $w$, $\beta_1$, and $\beta_2$; while $L_0$, $\alpha_0$ and $\beta_0$ are known. The unknown quantities are the distribution of $\theta$ and $d$. The sensor can construct $\Delta d$ if $\Delta\theta$ and $\Delta l$ are known from equation (5); further, it can reconstruct $\theta$ and $d$ if $\Delta\theta$ and $\Delta d$ are known. However, because the number of equations is small, the unknown values in equations (12) and (14) cannot be solved if $\theta$ equals $\theta+\Delta\theta$ and $l$ equals $l+\Delta l$. Here, we define

**Figure 4** Geometrical optics (Part): this is a part of Figure 3

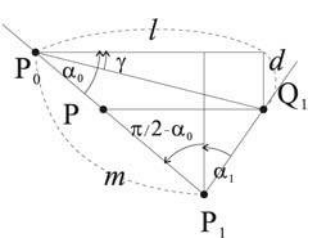

$$\Delta\alpha = \alpha_1 - \alpha_0 \tag{15}$$

From equation (12), we get

$$m^2\cos^2\Delta\alpha - (l^2 + d^2)(\cos^2(\alpha_0 + \Delta\alpha)) = 0 \tag{16}$$

When $\Delta\alpha$ is expressed as $\gamma = 0$, $\Delta\alpha \simeq 0$ from the second Taylor series expansion, $\Delta\alpha$ can be expressed as follows:

$$\begin{aligned}\Delta\alpha = \Big( & -(d^2+l^2)\cos\alpha_0\sin\alpha_0 \\ & \pm\sqrt{(d^2+l^2)^2\cos^2\alpha_0\sin^2\alpha_0 - (m^2-(d^2+l^2)\cos^2\alpha_0)} \\ & \times\sqrt{((-m^2)+(d^2+l^2)(\cos^2\alpha_0-\sin^2\alpha_0))}\Big) \Big/ (-m^2) \\ & +(d^2+l^2)(\cos^2\alpha_0-\sin^2\alpha_0)\end{aligned} \tag{17}$$

From equations (9), (15) and (17), we can express $\theta_1$ with the known parameters and measured values.

By defining $Q_1$ in equation (5) as the $n$th characteristic point and defining $\Delta d$ as $\Delta d_n$ from the continuation property of a boundary surface, we can assume that:

$$\Delta d_n \simeq \Delta d_{n+1} \tag{18}$$

Based on this assumption, we can express equation (5) as follows:

$$\Delta d_{n+1} = \frac{\Delta l_n}{\Delta\theta_n}\log\left(\left|\frac{\cos\theta_n}{\cos(\theta_n+\Delta\theta_n)}\right|\right) \tag{19}$$

Since, we assume that $d = 0$ at $l = 0$ and $l = L_0$, we obtain $l_n$ and $\theta_n$ from equation (12). We obtain $\Delta\theta_n$ from the given value of $\theta_n$ and calculate $\Delta d_{n+1}$ in equation (19). We obtain $\alpha_n$, $d_n$, and the distribution of $\alpha$ and $d$ by iterating this calculation step-by-step.

## 3. Simulations

### 3.1 Needle-shaped surface

We assume the upside-down needle-shaped surface shown in Figure 5 as the reflecting surface; further, $\beta_1 = \beta_2 = \beta_0$, $L_0 = 1{,}637$, and $\alpha_0 = \beta_0 = \pi/4$; the camera center is assumed to be at infinity. The calculation results are shown in Figures 6 and 7.

In both the Figures 6 and 7, the solid line represents the shape of the original reflection surface; the "–" curve represents the results of the summation of $\Delta l$ and $\Delta d$ from

**Figure 5** Needle-shaped deformation: in the simulation, the deformation of the reflection surface gives rise to this shape

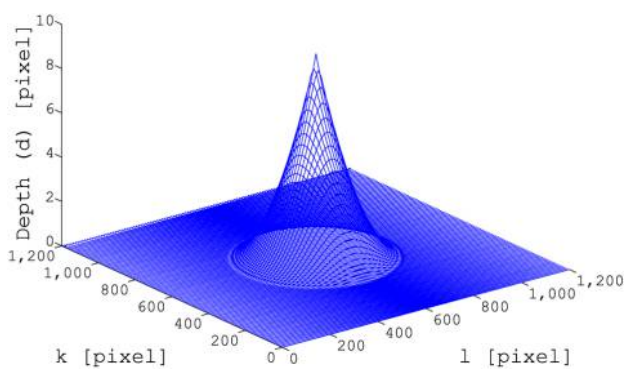


**Figure 6** Simulation results of $\theta$: the distribution of $\theta$ can be traced almost precisely

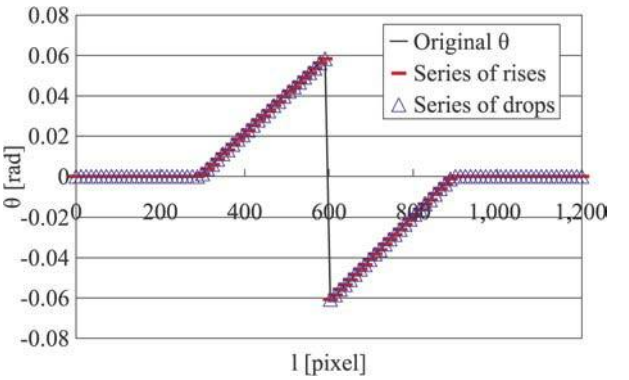


**Figure 7** Simulation results of depth ($d$): the distribution of depth ($d$) can be traced almost precisely

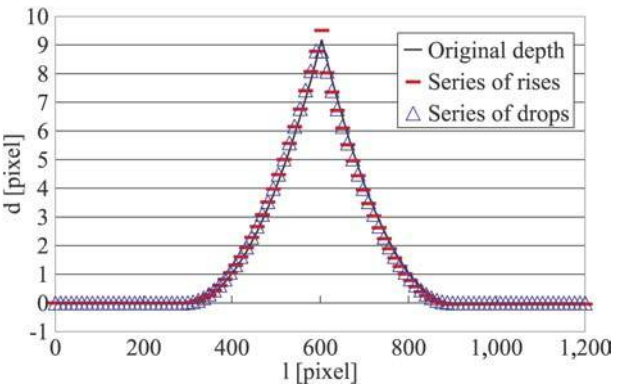


$l = 0$ in a series of rises. The "Δ" curve is the results of the summation from $l = L_0$ in a series of drops, and the "○" curve is the average of "–" and "Δ". It can be observed that the distribution of $d$ can be traced almost precisely.

We now examine the error in the true value in detail. Figures 8 and 9 shows the error distributions of $\theta$ and $d$, respectively. The error rate (the error/truth value) is suppressed to approximately 1 percent over the entire area. The error rate is caused by the approximation in equation (18) and $\Delta\alpha \simeq 0$.

**Figure 8** Simulation error results of $\theta$: the error of $\theta$ is suppressed under 0.0008 rad

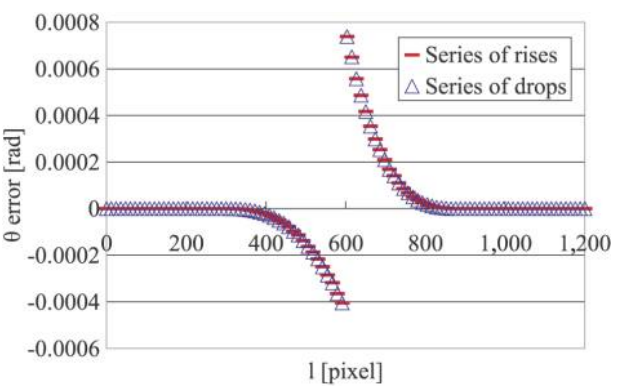

**Figure 9** Simulation error results of depth (*d*): the error of depth (*d*) is suppressed under 0.4 pixel

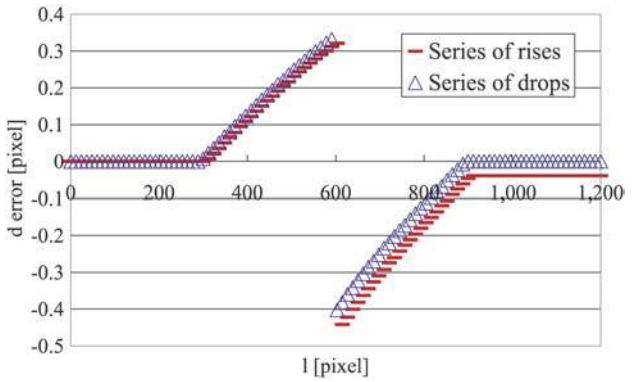


## 4. Implementation

Based on the simulation above described we built a real system. By using the developed sensor, we measured a real transformation in a real environment.

### 4.1 Silicone rubber with image pattern

The sensor uses the addition-polymerization-type silicone rubber (KE109A, B, Shin-Etsu Chemical Co., Ltd, www.silicone.jp/e/products/liquid/index.shtml). The Young's modulus of silicone is maintained at approximately about 1.6 MPa. We prepare a triangular pole-shaped flask with transparent acryl, pour silicone rubber into it and perform a lap reaction. After the lap reaction, we exfoliate using an acryl board and prepare the reflection surface. One of the left acryl surfaces on the left becomes the pattern surface and another one becomes the captured surface. In this case, we use a lattice-patterned paper as the pattern surface. In this manner, we prepare a sensor with a flexible mirror surface (Figure 10).

**Figure 10** Silicone rubber with a lattice pattern: the rubber is transparent and the pattern can be seen. The sensor is almost a cube-shaped with a side length of 60 mm

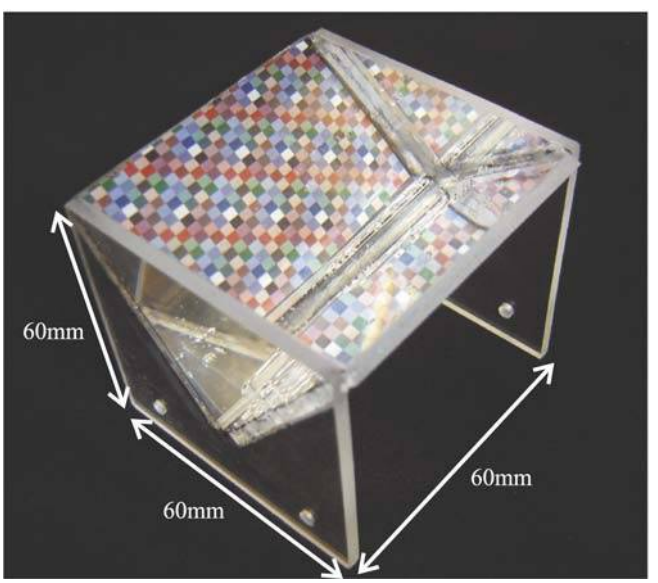


We install a camera to capture the flexible mirror surface adequately and fix it (Figure 11).

## 5. Experiments

The measurement procedure with the developed sensor is as follows. The tip of a pencil is pressed down onto the face of the sensor (Figure 12) by about 0.2 mm using a height gauge and the status is measured.

The images acquired before and after the deformation are shown in Figures 13 and 14. Here, we use a lattice pattern as the image pattern. We consider the association between one line of the central vertical lattice points from two pieces of images. By using equations (17) and (19), the shape is reconstructed. Figure 15 shows the mean values of the series of rises and series of drops. The scale of the image is 1 pixel $\simeq$ 0.1 mm because the size of the acquired image 625 × 392 pixel, the width of the lattice pattern is 2.5 mm width, and there are 16 pieces of the lattice in the vertical orientation of the image. Further, the peak value in Figure 15 is almost close to the true value. The error rate (the error/truth value) is suppressed to approximately 10 percent at the

**Figure 11** Overview of the sensor: the optic axis of the camera is located perpendicular to the captured surface

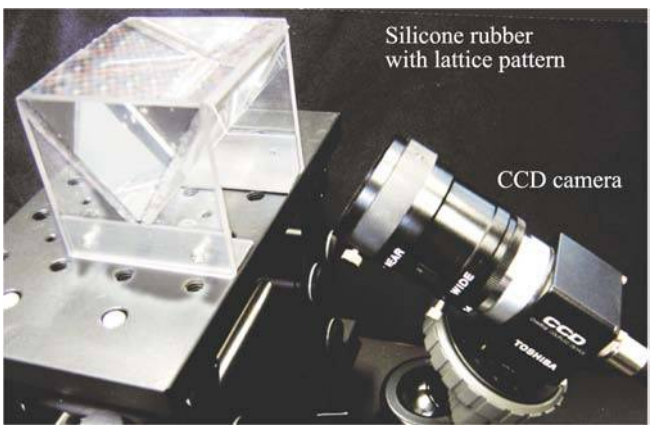


**Figure 12** Transform overview: a pencil is pressed down about 0.2 mm by using a height gauge

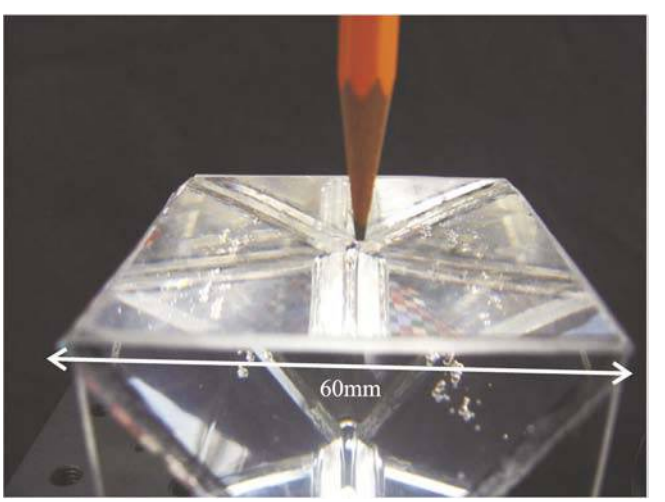

**Figure 13** Before deformation: the yellow marked points are used for the reconstruction

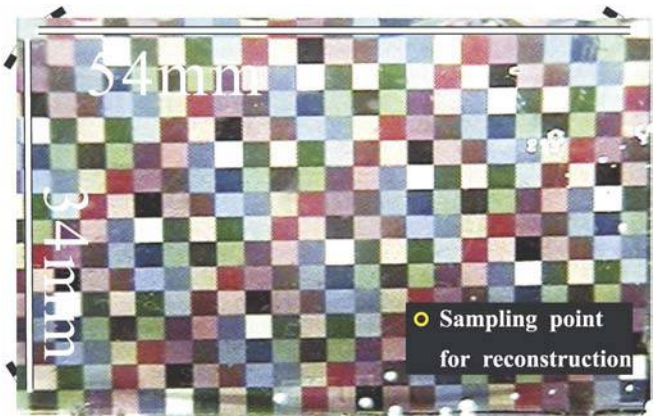


**Figure 14** After deformation: the yellow marked points are used for the reconstruction

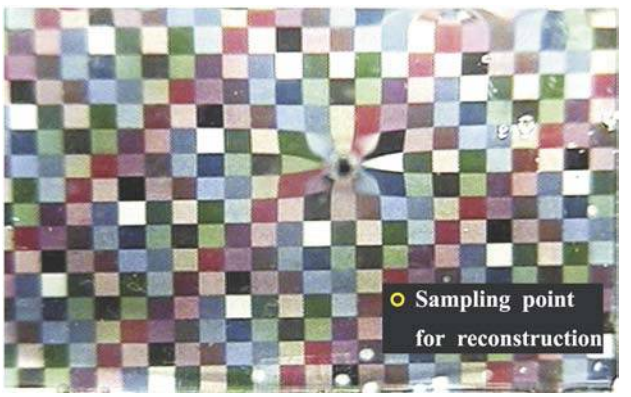


**Figure 15** Results of depth (*d*) measurement: the peak value is almost near the true value

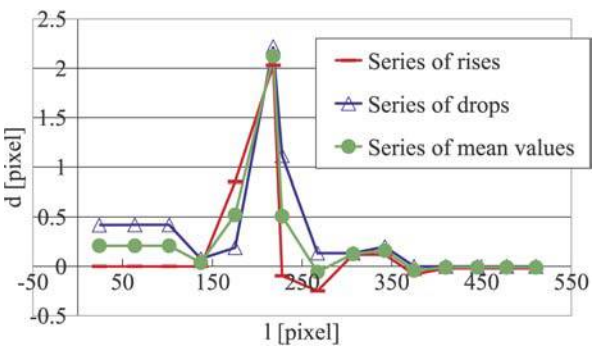


peak area. The value of $l = 0$ is near the true value in the series of rises, and $l = L_0$ is near the true value in the series of drops. This is caused by the accumulation of errors generated by the finite sum process. Comparing with the simulation, it is observed that the error rate increases. This is caused by the use of integer values of the pixel. This time, we manually acquire the corresponding points although the use of subpixel value is quite simple with some image processing algorithms. In the future; we aim to increase the accuracy, especially in terms of the error in the finite sum process.

## 6. Drawbacks and benefits

The sensor is made using very low cost materials. Owing to its simplicity and transparency, its combination with other devices offers many benefits; however, there are some drawbacks described below. These are some examples of the drawbacks and benefits.

### 6.1 Large deformation

In the Section 2.3, this time we assume a small deformation and use approximate equations. Therefore, if a large deformation occurs on the reflection surface, the approximate condition breaks. Though the deformed direction of the surface is limited (press only) and the deformation of the reflection image is also limited to some extent. Therefore, with some other approximation the sensor can re-construct the large deformation in the approximate condition.

### 6.2 Broad planar contact

Our sensor cannot detect a deformation when a broad planar shape is pressed on to the sensor. The sensor uses the distribution of the refractive index at the boundary of silicone rubber and air. If the boundary condition changes with the contact with an object, the reflection property changes simultaneously at the contact point. Therefore, if the contact point becomes a broader planar than the reflection surface, the reflection property of the entire sensor field will change and no reflection image will be acquired. However, if a sensor with a curved surface can used and the equation for the sensor can be solved, this drawback will be eliminated.

### 6.3 Multi sensing

Our sensor uses the distribution of the refractive index at the boundary of silicone rubber and air. As stated in the previous section, this is a drawback on one hand because the loss of the information occurs at the point of contact. On the other hand, this change enables the multi sensing of the surface deformation and the contact surface shape (Figure 16). For example, if a finger is pressed to this sensor, it can sense the deformation on the basis of the pressed force around the contact point and the shape of the fingerprint at the contact point.

**Figure 16** Multi sensing: the change in the boundary condition enables the sensor to detect the deformation and the contact surface shape simultaneously

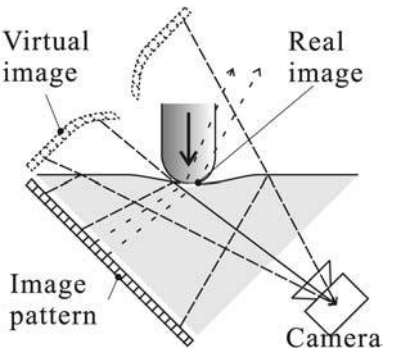


### 6.4 Contactless sensing and interactive device

Since,our sensor uses the transparent silicone rubber, light can pass without dispersing. If there is another camera facing the upper side, the camera can sense the remote visual information for an object without any contact between the sensor and the object (Figure 17). Using this information, the sensor can detect an oncoming object and the size of the object, and it can stand by for the contact.

Another benefit of using transparency is that we can design an interactive device using a projector and a screen (Figure 18). By using a cloth-type screen, the sensor can sense the deformation and display an image simultaneously. This is because the contact points of the cloth and the sensor are discrete; the sensor works without being influenced by a projector.

### 6.5 Sensing with active patterns

By using a liquid crystal display (LCD) instead of the image pattern, the sensor can use the feedback sensing method. In other words, if the deformation occurs when there is contact with an object, the sensor can change the image pattern in order to cancel the deformation of the virtual image. In this way, the zero method can be used with the sensor. The zero method will cause the sensor to detect smaller changes on the reflection surface. Furthermore, the zero method enables the sensor to control the reflection image. Therefore, if the resolution of the reflection image matches that of the camera, the sensor can utilize the camera resolution to the maximum possible extent.

**Figure 17** Contactless sensing: the lower camera can detect objects that did not touch the sensor

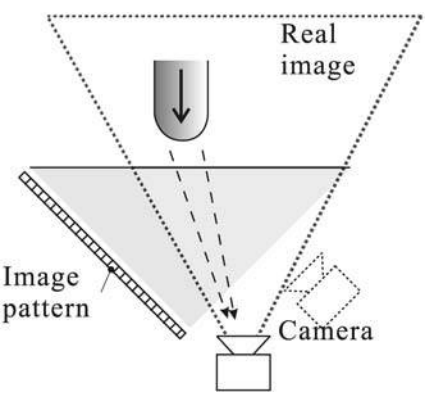


**Figure 18** Interactive device: the transparency and the projector cause the sensor to sense the deformation and act as a display simultaneously

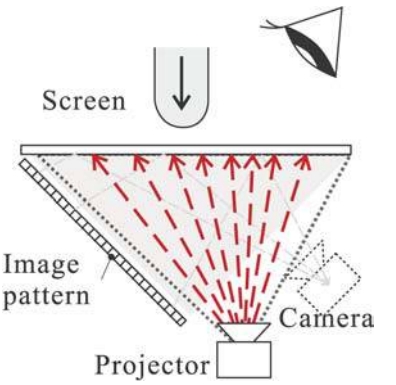


### 6.6 Thin device and fast sensing

By using a saw-shaped rubber (Figure 19) instead of a prism-shaped one, we can design a thin sensor device with this method. In addition, by using light emission diodes (LEDs) and photodetectors (PDs) to form the image pattern and as the camera, we can design a fast data-acquiring active sensor.

### 6.7 Lighting

This sensor uses only diffused light from the pattern surface; therefore, the lights must reach to the pattern surface. Further due to the transparency of the sensor, light from the outer environment can be used. Even if the outer environment is dark, the light from the camera position brightens the pattern surface because of the flexible mirror surface. Furthermore, if an LCD display is used for the pattern surface, the light from the LCD display generates an environment that is sufficiently bright to capture the surface.

## 7. Conclusion

In this paper, we have proposed a tactile sensor that utilizes the principle of an optical lever and a flexible reflection surface. We have designed a tactile sensor that takes advantage of the reflection image whose deformation was detected with high precision using an optical lever; the sensor also takes sufficient advantage of the resolution of a camera by using transparent silicone rubber as a flexible mirror surface.

On the basis of a simulation, we have shown that the reconstruction of a reflection plane of reflection from an image is possible. The reconstruction is carried out by using geometrical optics and by an appropriate approximation in the constituted tactile sensor. In addition, we have produced a prototype made of silicone rubber and have shown that the shape restoration of a reflection plane is possible. With regard to the resolution, humans can detect a displacement of

**Figure 19** Thin device and fast sensing: the saw shape results in a thin sensor, and the use of LEDs and PDs results in a fast sensor

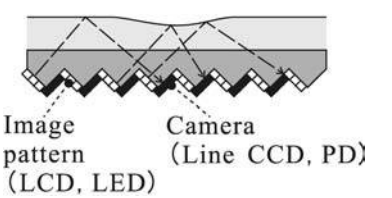

0.1 mm (Freeman and Johnson, 1982). On the other hand, the prototype of the sensor can quantify a displacement of 0.2 mm displacement. Furthermore, due to the optical lever, the further the camera is placed the more the displacement can be amplified. We then showed the drawbacks and benefits of this sensor.

Our proposed technique combines an optical lever and a flexible surface of reflection. Therefore, the modification of a pattern surface and a captured surface in accordance with the measured object is possible. Although the sensor can have varied application, our target application is a sensing tool for determining contact status. For example, its use in the quantification of the contact status on rubbing a towel or a brush is appropriate for the sensor. In the future, we will examine these combinations, in particular, dynamic pattern generation using an LCD for more precise sensing.

## References

Baba, M., Konishi, T. and Handa, H. (2002), "Shape measurement of columnar objects with specular surfaces by slit ray projection method", *Systems and Computers in Japan*, Vol. 33 No. 4, pp. 50-60.

Begej, S. (1984), "An optical tactile array sensor", *SPIE Intelligent Robotics and Computer Vision*, Vol. 521, pp. 271-80.

Freeman, A.W. and Johnson, K.O. (1982), "A model accounting for effects of vibratory amplitude on responses of cutaneous mechanoreceptors in macaque monkey", *Journal of Physiology*, Vol. 323, pp. 43-64.

Kamiyama, K., Vlack, K., Kajimoto, H., Kawakami, N. and Tachi, S. (2005), "Vision-based sensor for real-time measuring of surface traction fields", *IEEE Computer Graphics & Applications Magazine*, pp. 68-75.

Massig, J.H. (2001), "Deformation measurement on specular surfaces by simple means", *Optical Engineering*, Vol. 40 No. 10, pp. 2315-8.

Meyer, G. and Amer, N.M. (1988), "Novel optical approach to atomic force microscopy", *Applied Physics Letters*, Vol. 53 No. 12, pp. 1045-7.

Miike, H., Koga, K., Yamada, T., Kawamura, T., Kitou, M. and Takikawa, N. (1995), "Measuring surface shape from specular reflection image sequence – quantitative evaluation of surface defects of plastic moldings", *Japanese Journal of Applied Physics, Part 2*, Vol. 34 No. 12A, pp. L1625-8.

Schultz, H.J. (1992), "Specular surface stereo: a new method for retrieving the shape of a water surface", *Proceedings of SPIE – The International Society for Optical Engineering*, Vol. 1749, pp. 283-94.

Yamada, K., Goto, K., Nakajima, Y., Koshida, N. and Shinoda, H. (2002), "A sensor skin using wire-free tactile sensing elements based on optical connection", *SICE 2002. Proceedings of the 41st SICE Annual Conference*, The Society of Instrument and Control Engineers, Tokyo.

Yamaguchi, I., Yamamoto, A. and Yano, M. (1999), "Surface topography by wavelength scanning interferometry", *Optical Engineering*, Vol. 39 No. 1, pp. 40-6.

## Corresponding author

**Satoshi Saga** can be contacted at: satoshi_saga@ipc.i.u-tokyo.ac.jp

**This article has been cited by:**


1. Ryo Akiyama, Kazuto Kamiyama, Masaru Kojima, Mitsuhiro Horade, Yasushi Mae, Tatsuo AraiDevelopment of multi-functional robot hand for multi-legged robot 220-225. [CrossRef]
2. Kazuhiro Shimonomura, Hiroto Nakashima, Kentaro NozuRobotic grasp control with high-resolution combined tactile and proximity sensing 138-143. [CrossRef]
3. Thi-Trang Tran, Cheolkeun HaSlippage Estimation Using Sensor Fusion 471-481. [CrossRef]
4. Kai-Wei Liao, Max T. Hou, Hiroyuki Fujita, J. Andrew Yeh. 2015. Liquid-based tactile sensing array with adjustable sensing range and sensitivity by using dielectric liquid. *Sensors and Actuators A: Physical* **231**, 15-20. [CrossRef]
5. Eric V Eason, Elliot W Hawkes, Marc Windheim, David L Christensen, Thomas Libby, Mark R Cutkosky. 2015. Stress distribution and contact area measurements of a gecko toe using a high-resolution tactile sensor. *Bioinspiration & Biomimetics* **10**:1, 016013. [CrossRef]
6. Yuji Ito, Youngwoo Kim, Goro Obinata. 2014. Contact Region Estimation Based on a Vision-Based Tactile Sensor Using a Deformable Touchpad. *Sensors* **14**:4, 5805-5822. [CrossRef]
7. Y. Ito, G. Obinata, Y. Kim, C. NagaiMultimodal Sensing by a Vision-Based Tactile Sensor Using a Deformable Touchpad 515-538. [CrossRef]
8. Mallory L. Hammock, Alex Chortos, Benjamin C.-K. Tee, Jeffrey B.-H. Tok, Zhenan Bao. 2013. 25th Anniversary Article: The Evolution of Electronic Skin (E-Skin): A Brief History, Design Considerations, and Recent Progress. *Advanced Materials* **25**:42, 5997-6038. [CrossRef]
9. Alessandro Massaro, Fabrizio Spano, Paolo Cazzato, Carola La Tegola, Roberto Cingolani, Athanassia Athanassiou. 2013. Robot Tactile Sensing: Gold Nanocomposites As Highly Sensitive Real-Time Optical Pressure Sensors. *IEEE Robotics & Automation Magazine* **20**:2, 82-90. [CrossRef]
10. Jianxin Liu, Xuan Zhang, Zhiming Li, Xuling Li. 2013. A Tent Map Based A / D Conversion Circuit for Robot Tactile Sensor. *Journal of Sensors* **2013**, 1-5. [CrossRef]
11. Stephen Williams, Lonnie Parker, Ayanna Howard. 2012. Terrain Reconstruction of Glacial Surfaces : Robotic Surveying Techniques. *IEEE Robotics & Automation Magazine* **19**:4, 59-71. [CrossRef]
12. Yuji Ito, Youngwoo Kim, Chikara Nagai, Goro Obinata. 2012. Vision-Based Tactile Sensing and Shape Estimation Using a Fluid-Type Touchpad. *IEEE Transactions on Automation Science and Engineering* **9**:4, 734-744. [CrossRef]
13. A. YaoDepartment of Electronic and Electrical Engineering, University of Bath, Bath, UK M. SoleimaniDepartment of Electronic and Electrical Engineering, University of Bath, Bath, UK. 2012. A pressure mapping imaging device based on electrical impedance tomography of conductive fabrics. *Sensor Review* **32**:4, 310-317. [Abstract] [Full Text] [PDF]
14. Xuefeng ZhangState Key Laboratory for Mechanical Manufacturing Systems Engineering, Xi'an Jiaotong University, Xi'an, China Yulong ZhaoState Key Laboratory for Mechanical Manufacturing Systems Engineering, Xi'an Jiaotong University, Xi'an, China Xuelei ZhangState Key Laboratory for Mechanical Manufacturing Systems Engineering, Xi'an Jiaotong University, Xi'an, China. 2012. Design and fabrication of a thin and soft tactile force sensor array based on conductive rubber. *Sensor Review* **32**:4, 273-279. [Abstract] [Full Text] [PDF]
15. Tomoaki Yoshikai, Marika Hayashi, Yui Ishizaka, Hiroko Fukushima, Asuka Kadowaki, Takashi Sagisaka, Kazuya Kobayashi, Iori Kumagai, Masayuki Inaba. 2012. Development of Robots with Soft Sensor Flesh for Achieving Close Interaction Behavior. *Advances in Artificial Intelligence* **2012**, 1-27. [CrossRef]
16. Yuji Ito, Youngwoo Kim, Goro Obinata. 2011. Robust Slippage Degree Estimation Based on Reference Update of Vision-Based Tactile Sensor. *IEEE Sensors Journal* **11**:9, 2037-2047. [CrossRef]
17. Jong-Ha Lee, Chang-Hee Won. 2011. High-Resolution Tactile Imaging Sensor Using Total Internal Reflection and Nonrigid Pattern Matching Algorithm. *IEEE Sensors Journal* **11**:9, 2084-2093. [CrossRef]
18. Yuji Ito, Youngwoo Kim, Chikara Nagai, Goro Obinata. 2011. Contact State Estimation by Vision-Based Tactile Sensors for Dexterous Manipulation with Robot Hands Based on Shape-Sensing. *International Journal of Advanced Robotic Systems* **8**:4, 54. [CrossRef]
19. Y. Tanaka, Y. Horita, A. Sano, H. FujimotoTactile sensing utilizing human tactile perception 621-626. [CrossRef]
20. M. Koike, S. Saga, T. Okatani, K. DeguchiSensing method of total-internal-reflection-based tactile sensor 615-619. [CrossRef]
21. Y Ito, Y Kim, C Nagai, G ObinataAcquisition of tactile information by vision-based tactile sensor for dexterous handling of robot hands 891-896. [CrossRef]

22. Yuji Ito, Youngwoo Kim, Chikara Nagai, Goro ObinataShape sensing by vision-based tactile sensor for dexterous handling of robot hands 574-579. [CrossRef]
23. Ali Mohammad Shariatmadar Ahmadi, Mohammad Javad Shamsollahi, Alireza Mirbagheri, Farzam FarahmandDesign, optimization and experimental evaluation of a novel tactile sensor for large surgical grasper V2-111-V2-116. [CrossRef]
24. K. Sato, K. Kamiyama, N. Kawakami, S. Tachi. 2010. Finger-Shaped GelForce: Sensor for Measuring Surface Traction Fields for Robotic Hand. *IEEE Transactions on Haptics* **3**:1, 37-47. [CrossRef]
25. Tomoaki Yoshikai, Marika Hayashi, Asuka Kadowaki, Takefumi Goto, Masayuki InabaDesign and development of a humanoid with Soft 3D-deformable sensor flesh and automatic recoverable mechanical overload protection mechanism 4977-4983. [CrossRef]
26. Satoshi Saga, Masashi Konyo, Koichiro DeguchiComparison of spatial and temporal characteristic between reflection-type tactile sensor and human cutaneous sensation 22-27. [CrossRef]